Bioinformatics analysis identification of *AKT3* and *RAC1* as key genes in postmenopausal osteoporosis

LIYONG ZHANG[1*], XIAOMING LI[2*], CHUNFEI WAN[1], WEIWEI DA[1], JUN ZHANG[1], LIHONG FAN[1], QIANG FU[1], SHUNMIN XING[2] and YONGXIANG WANG[3]

[1]Department of Orthopedics, Yangzhou Hospital of Traditional Chinese Medicine, Clinical Traditional Chinese Medical College of Yangzhou University, Hanjiang, Yangzhou 225012; [2]Department of Orthopedics, 72nd Group Military Hospital, Wuxing, Huzhou, Zhejiang 313000; [3]Department of Orthopedics, Subei People's Hospital of Jiangsu Province, Clinical Medical College of Yangzhou University, Hanjiang, Yangzhou 225001, P.R. China

Received September 12, 2021; Accepted March 10, 2022

DOI: 10.3892/etm.2022.11592

Abstract. Postmenopausal osteoporosis (PMO) is an aging-associated disease that manifests as degradation of bone tissue microstructure leading to decreased bone mass and increased bone fragility. Differentiation of peripheral blood mononuclear cells into osteoclasts is an important process in the development of PMO and identification of key genes that drive differentiation is essential to reveal the mechanism of PMO. The present study combined bioinformatics analysis of a Gene Expression Omnibus dataset of PMO and drug (bisphosphonate) target prediction using the STITCH database to identify hub genes in patients with PMO. Next, the expression of candidate hub genes was assessed in osteoclasts differentiated from THP-1 cells and small interfering RNA assays were performed to assess the function of selected hub genes. The present study identified 10 hub genes including *WNT1, AKT3*, disheveled segment polarity protein 1, cyclin D1, H2B clustered histone 17, *JUN, EGFR, RAC1*, actinin α1 *(ACTN1)* and *ACTN2*. Among these, *AKT3* and *RAC1* were highly upregulated during osteoclast differentiation, and knockdown of AKT3 and RAC1 using small interfering RNA enhanced the inhibitory effect of bisphosphonates on osteoclast differentiation and apoptosis of monocytes as assessed by tartrate-resistant acid phosphatase staining and flow cytometry examining Annexin V-FITC/PI staining, respectively. In conclusion, *AKT3* and *RAC1* were key for development of PMO and inhibiting *AKT3* and *RAC1* may improve the therapeutic efficacy of bisphosphonates.

Correspondence to: Professor Yongxiang Wang, Department of Orthopedics, Subei People's Hospital of Jiangsu Province, Clinical Medical College of Yangzhou University, 196 West Huayang Road, Hanjiang, Yangzhou 225001, P.R. China
E-mail: wang_yx2011@yeah.net

Professor Shunmin Xing, Department of Orthopedics, 72nd Group Military Hospital, 9 Chezhan Road, Huzhou, Zhejiang 313000, P.R. China
E-mail: sm58_zhejiangx@126.com

*Contributed equally

Key words: postmenopausal osteoporosis, bioinformatics, bisphosphonates, AKT3, RAC1, osteoclast, peripheral blood mononuclear cells

Introduction

Postmenopausal osteoporosis (PMO) is an aging-associated disease that manifests as degradation of bone tissue microstructure leading to decreased bone mass and increased bone fragility (1). Decreased estrogen levels are the primary factor for onset of PMO (2). According to a previous study, approximately one-third of women aged 60-70 years have from osteoporosis worldwide and nearly one-third of women >50 years of age develop osteoporotic fractures (3). Therefore, understanding the pathogenesis of PMO is key for its prevention and treatment.

The primary pathogenic feature of PMO is imbalance between bone resorption and formation, wherein the rate of bone resorption by osteoclasts exceeds the rate of bone formation by osteoblasts (4). Peripheral blood mononuclear cells (PBMCs) directly participate in osteoclast formation. PBMCs are precursors of osteoclasts (5) and secrete osteoclast-inducing factors such as interleukin-1 (IL-1), IL-6 and tumor necrosis factor-α (TNF-α) (6). Human PBMCs express genes associated with osteoporosis, including annexin A1, S100 calcium-binding protein A4 and transmembrane protein 64 (7). The discovery of such genes provides novel clues to understand the pathogenesis of PMO.

To identify novel and hub genes of PMO, the present study performed joint bioinformatics analysis including screening of differentially expressed genes (DEGs) from Gene Expression Omnibus (GEO) dataset and identification of targets of bisphosphonates (a bone resorption inhibitor widely used in the clinic) (8) from the STITCH database. *In vitro* experiments were performed to verify the role of hub genes in differentiation of mononuclear macrophage into osteoclasts.

Materials and methods

Cell culture and induced differentiation of osteoclasts. The human monocyte cell line THP-1 was purchased from Santa Cruz Biotechnology, Inc. (cat. no. sc-7274, USA) and maintained in RPMI-1640 medium (HyClone; Cytiva) supplemented with 10% FBS (Gibco; Thermo Fisher Scientific, Inc.). Cells were cultured in an incubator under 5% CO_2 at 37˚C. As described previously (9), THP-1 cells were seeded in a 24-well plate ($1x10^6$ cells/well). The next day, cells were treated with 1,000 units of macrophage-colony-stimulating factor (M-CSF; R&D Systems, Inc.), 5 ng/ml phorbol 12-myristate 13-acetate (LGC Standards Ltd.) and 50 ng/ml soluble receptor activator of NF-κB ligand (sRANKL; MedChemExpress). At 3 and 5 days, the formation of osteoclasts was confirmed by morphological determination of coenocytes and tartrate-resistant acid phosphatase staining (TRAP staining). TRAP staining was performed according to the manufacturer's protocol (Wuhan Servicebio Technology Co., Ltd.). Briefly, after induced differentiation into osteoclast, the THP-1 cells were fixed using 4% paraformaldehyde for 20 min at room temperature. After washing, THP-1 cells were treated with TRAP dyeing liquor (Wuhan Servicebio Technology Co., Ltd.) for 2 h at room temperature. Next, the TRAP dyeing liquor was removed and THP-1 cells were washed, then hematoxylin dye was used for nuclear staining for 15 sec at room temperature. Finally, the nuclear fusions were observed under a light microscope (Nikon Eclipse E100; Nikon Corporation) and the fusion rate of multinuclear cells that indicates the formation of osteoclast was quantified by ImageJ software (version 1.8.0; National Institutes of Health).

Small interfering (si)RNA synthesis and transfection. siRNAs targeting *AKT3* and *RAC1* were designed and synthesized by Jiman Biotechnology (Shanghai) Co., Ltd. with the following target sequences: siRNA-AKT3, 5'-CAGCAGGCACGUUAA CUCGAA-3' and siRNA-RAC1, 5'-AACCUUUGUACG CUUUGCUCA-3'. All sequences of siRNAs are presented in Table SI. Negative control (NC) siRNAs with no homology to siRNA-AKT3 and siRNA-RAC1 were designed and synthesized by Jiman Biotechnology (Shanghai) Co., Ltd. as follows: siRNA-NC, 5'-UUCUCCGAACGUGUCACGU-3'. siRNA transfection was performed using Lipofectamine® 2000 (Invitrogen: Thermo Fisher Scientific, Inc.) according to the manufacturer's instructions. Briefly, THP-1 cells in the logarithmic growth phase were seeded at $5x10^4$ cells/well in a 24-well plate and cultured at 37˚C for 24 h. The RPMI-1640 medium (HyClone; Cytiva) was replaced with serum-free Opti-MEM (Thermo Fisher Scientific, Inc.) and cells were transfected at 37˚C with lipofectamine 2000 (1:100) and 100 nmol/l siRNA for 20 min for fluorescence-siRNA-transfection reagent mixture formation. Subsequently, serum-free Opti-MEM was added to a total volume of 500 μl, and THP-1 cells were cultured in an incubator for 4-6 h. Finally, the transfection efficiency was assessed by detecting expression of objective proteins by western blotting. Cells treated with liposomes (cell:liposome, 1:100) and siRNA-NC at 37˚C were used as NC. At 6 h post-transfection, the medium was replaced with RPMI-1640 (HyClone; Cytiva) with 10% FBS (Gibco; Thermo Fisher Scientific, Inc.) and cells were cultured at 37˚C for 48 h before being harvested for western blotting.

Apoptosis analysis. Annexin V-FITC/PI Cell Apoptosis Detection kit (TransGen Biotech Co., Ltd.) was used to detect apoptotic cells. The apoptosis rate was calculated as the early apoptosis rate (lower right quadrant) plus the late apoptosis rate (upper right quadrant). Following bisphosphonate (10 μM) treatments for 24 h at room temperature, THP-1 cells were detached by EDTA-free trypsin digestion and collected by centrifugation at 4˚C at 201 x g for 5 min. The cells were re-suspended in PBS and collected by centrifugation at 4˚C at 201 x g for 5 min. The cells were re-suspended in 100 μl binding buffer, mixed with 5 μl Annexin V-FITC reagent, and placed in the dark at room temperature for 15 min. Cell suspension was mixed with 5 μl PI, incubated at room temperature for 5 min and subjected to flow cytometry analysis. The supplier of flow cytometer (CytoFLEX S) was Beckman Coulter, Inc., and the analysis software was CytExpert (version 2.0; Beckman Coulter, Inc.).

Cell viability assay. THP-1 cells were plated in a 96-well plate (8,000 cells/well) and treated with pamidronate at various concentrations (1, 2.5, 5, 10, 20, 50 and 100 μM) at 37˚C for 24 h. The cells were washed with PBS and incubated with 100 μl RPMI-1640 medium (HyClone; Cytiva) containing CCK-8 reagent (Dongren Chemical Technology) for 1-4 h. Cell viability was measured by absorbance at 450 nm using a microplate reader.

Reverse transcription-quantitative (RT-q)PCR. Total RNA of cells was isolated using a Total RNA Extraction kit (Beijing Solarbio Science & Technology Co., Ltd.) and 100 ng RNA was used for RT-qPCR assay using a Two-Step qPCR SuperMix (Beijing Transgen Biotech Co., Ltd.). The procedure of reverse transcription was as follows: A temperature program of 5-min priming at 25˚C followed by reverse transcription at 42˚C for 30 min and reverse transcription inactivation at 85˚C for 5 min was run. After a final cool-down to 4˚C, the cDNA was stored at -80˚C for subsequent use. The amplification conditions were as follows: Pre-denaturation at 95˚C for 10 min, followed by 40 cycles of denaturation at 95˚C for 30 sec, annealing at 56˚C for 30 sec and extension at 72˚C for 45 sec. The qPCR data were analyzed by the $\Delta\Delta C$q method (10). *GAPDH* was used as an internal reference gene as previously described (11). The sequence information of the primers is provided in Table SII.

Retrieval of PMO gene expression profiles from GEO database. The raw data of PMO gene expression profiles were downloaded from National Center for Biotechnology Information-GEO database (ncbi.nlm.nih.gov). The selection criteria were as follows: Samples were from peripheral blood and the object of study was PBMCs. According to these criteria, one dataset (GEO accession no. GSE56815; ncbi.nlm.nih.gov/gds/?term=GSE56815) containing gene expression profiles of PBMCs from a cohort of 80 females was selected. The cohort included 40 cases each of pre- and post-menopausal patients, with each group containing 20 cases each of low and high bone mineral density (BMD). The gene expression profiling of this dataset was determined using the Affymetrix HG-133A array platform (Affymetrix; Thermo Fisher Scientific, Inc.). A heatmap was generated to indicate hierarchical clustering with the R language 'pheatmap' package (R version 4.1.2).

Prediction of bisphosphonates targets. Using the STITCH database (stitch.embl.de/cgi), predicted bisphosphonates targets were retrieved and a protein-protein interaction (PPI) network was constructed. Functional enrichment, including biological processes and KEGG pathways, of the network were analyzed using the STITCH database. The results were plotted using the ggplot2 2.2.1 package in RStudio (version 4.1.2) (12).

Identification of shared KEGG pathways between bisphosphonates targets and DEGs in PMO. The enriched KEGG pathways of the bisphosphonates-protein network were produced using STITCH database. The enrichment analysis of KEGG pathways of DEGs in the PMO dataset was conducted using Database for Annotation, Visualization and Integrated Discovery Bioinformatics Resources 6.8 (13). The shared KEGG pathways between the two analyses were obtained and displayed using Venn Diagram (version 2.1; ehbio.com/ImageGP/index.php/Home/Index/index.html).

Identification of hub genes. Cytoscape (version 3.6.0; https://cytoscape.org/) is a powerful visualization software, including add-on modules for protein interaction visual analysis, calculation and analysis of interaction network. The MCODE module in Cytoscape was used to weigh the connection between nodes. For each node in the interaction network of selected genes, two indices were selected to calculate topological features. 'Degree' was defined as the number of edges to node i; 'closeness' was the inverse of the sum of the distance from node i to other nodes. When applying the degree and closeness algorithm, proteins with degree >20 and closeness >48.8 were considered to be major hubs. Both the hub gene and network were retained, calculation data were downloaded, and the above indicators (degree and closeness algorithm) were sorted as previously described (14). Finally, the genes involved in the four common KEGG pathways, including 'pathways in cancer', 'HIF-1 signaling pathway', 'human T-cell leukemia virus 1 infection' and 'viral carcinogenesis', were filtered out and 10 genes that met the requirements (degree >20 and closeness >48.8) were selected.

Western blotting. The THP-1 cells were collected on ice and lysed with RIPA buffer (Roche Diagnostics) supplemented with protease inhibitor (Complete Mini Tablets; Roche Diagnostics) for 30 min at 4˚C with shaking. The cell lysate was centrifuged at 4˚C at 16,770 x g for 15 min and supernatant was collected. Protein was quantified using the BCA Protein Concentration Determination Kit (cat. no. P0012S; Beyotime Institute of Biotechnology). Equal amounts of protein (5 μg/lane) samples were mixed with loading buffer, denatured at 100˚C for 10 min and separated by SDS-PAGE (10%). The proteins were transferred onto PVDF membranes (Invitrogen; Thermo Fisher Scientific, Inc.) and blocked at room temperature with 5% non-fat dry milk for 1 h. The membranes were incubated overnight at 4˚C in solution containing primary antibodies (all Abcam) as follows: Anti-Akt3 (1:1,000; cat. no. ab152157), anti-Rac1 (1:1,000; cat. no. ab155938) and anti-GAPDH (1:2,000; cat. no. ab128915). Subsequently, blots were incubated with horseradish peroxidase-conjugated secondary antibody (1:3,000; cat. no. ab288151; Abcam) for 1 h at room temperature. Protein expression was detected with SuperSignal West Pico (Thermo Fisher Scientific, Inc.) using the ChemiDoc MP imaging system (Bio-Rad Laboratories, Inc.). Protein densitometry was quantified using Image Lab software (version 5.2.1; Bio-Rad Laboratories, Inc.).

Statistical analysis. GraphPad Prism 8.0 software (GraphPad Software, Inc.) was used for all statistical analysis. Normality test was performed before sample comparison (Shapiro-Wilk or D'Agostino and Pearson normality test). One-way analysis of variance followed by Tukey's post hoc test was used to compare ≥3 groups. Data are presented as the mean ± standard deviation. Every experiment was repeated three times. $P<0.05$ was considered to indicate a statistically significant difference (15).

Results

A total of 290 DEGs were screened from the GEO dataset in PMO. Based on the aforementioned selection criteria, the GEO dataset GSE56815 was selected and PBMC expression profiles from postmenopausal patients were extracted for DEG analysis. Between patients with high and low BMD, there were 290 DEGs, of which 104 genes were up- and 186 were downregulated in the low BMD group (Fig. 1A). The heatmap combined with the hierarchical clustering of DEGs was shown in Fig. 1B. The results demonstrated that most samples were discriminatively clustered as low BMD/high BMD. Overall, the gene profile of the low BMD group was markedly different from that in the high BMD group.

Functional annotation of DEGs in PMO. The selected 290 DEGs were subjected to functional annotation. GO enrichment analysis of the biological process showed that DEGs were primarily enriched for 'positive/negative regulation of transcription from RNA polymerase II', 'translational initiation' and 'MAPK cascade'. The cellular components were associated with 'cytoplasm' and molecular functions were associated with 'protein binding' and 'Poly(A) RNA binding'. These data demonstrated that PMO was associated with genes involved in RNA synthesis and regulation (Fig. 2A). In KEGG pathway analysis, the enriched pathways included 'endocytosis' and 'thyroid hormone signaling', indicating a connection between hormonal regulation and PMO (Fig. 2B). Overall, the functional annotation of DEGs in PMO indicated that most DEGs were closely associated with the process of DNA reproduction.

Bisphosphonates target analysis using the STITCH database and the interaction network. Using the STITCH database, functional partners of bisphosphonate were analyzed, which resulted in 16 candidates. The first cluster included 10 proteins, namely farnesyl diphosphate synthase, geranylgeranyl diphosphate synthase 1, intracisternal A particle-promoted polypeptide, IL6, MMP9, prostaglandin-endoperoxide synthase 2, MMP3, DNA methyltransferase 1, mannose receptor C type 2 and DNA polymerase β. The second cluster included IL-6ST, IL-6R, DNA methyltransferase 3α, DNA methyltransferase 3β, histone deacetylase 1 and proliferating cell nuclear antigen (Fig. 3A). The enrichment analysis showed that these molecules were associated with biological processes

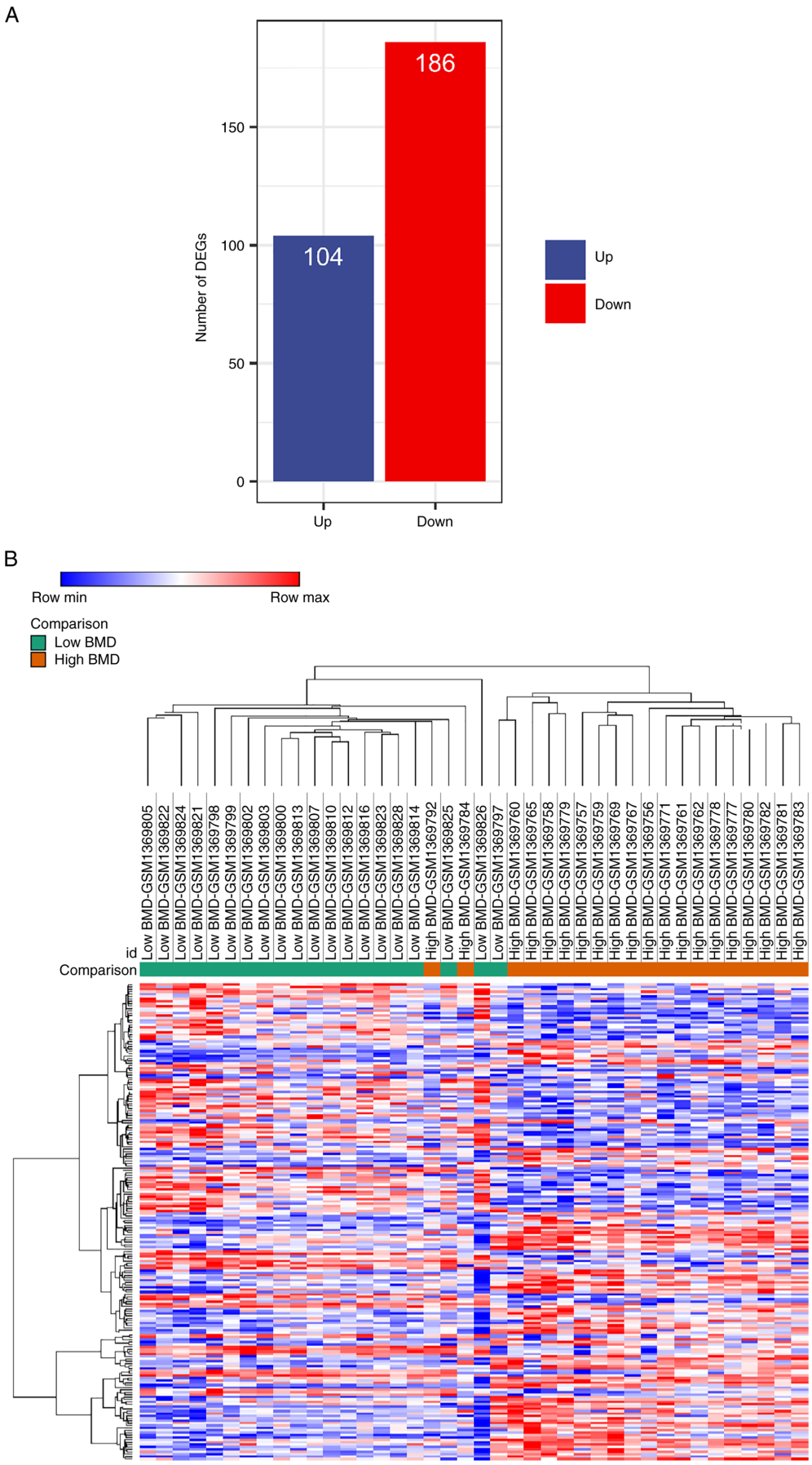

Figure 1. Differential gene expression analysis of patients with PMO. The gene expression profiles of peripheral blood mononuclear cells of patients with PMO were extracted from the Gene Expression Omnibus dataset GSE56815. (A) Raw expression data were normalized and log2 transformed and the numbers of DEGs are presented (low BMD vs. high BMD). (B) DEGs in patients with low vs. high BMD were visualized by heatmap with hierarchical clustering. PMO, postmenopausal osteoporosis; DEG, differentially expressed gene; BMD, bone mineral density.

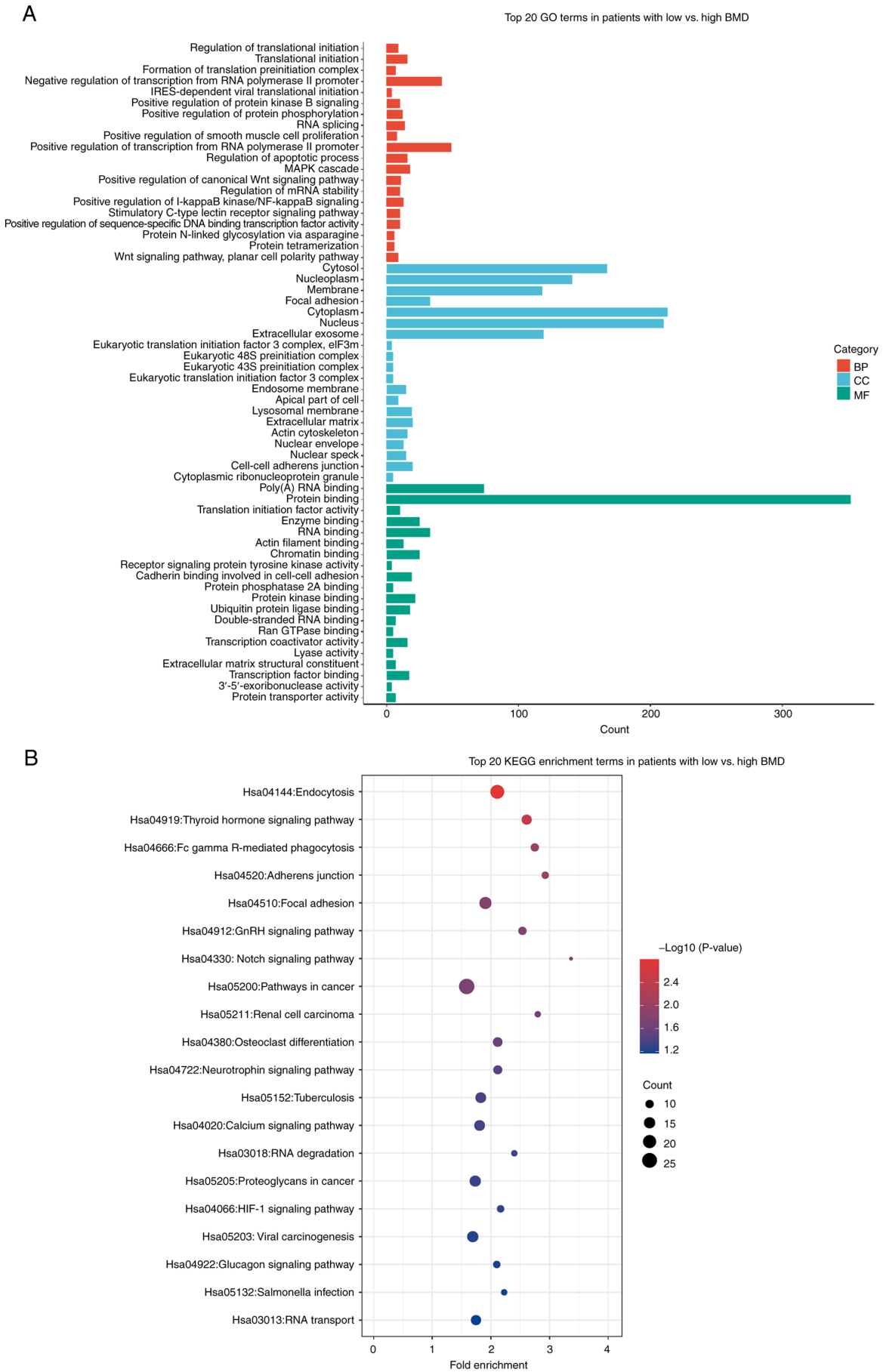

Figure 2. Functional annotation of DEGs in postmenopausal osteoporosis. By using Database for Annotation, Visualization and Integrated Discovery 6.8 online database, DEGs were subjected to (A) GO and (B) KEGG pathway enrichment analysis. DEG, differentially expressed gene; GO, Gene Ontology; KEGG, Kyoto Encyclopedia of Genes and Genomes; BP, biological process; CC, cellular component; MF, molecular function; BMD, bone mineral density.

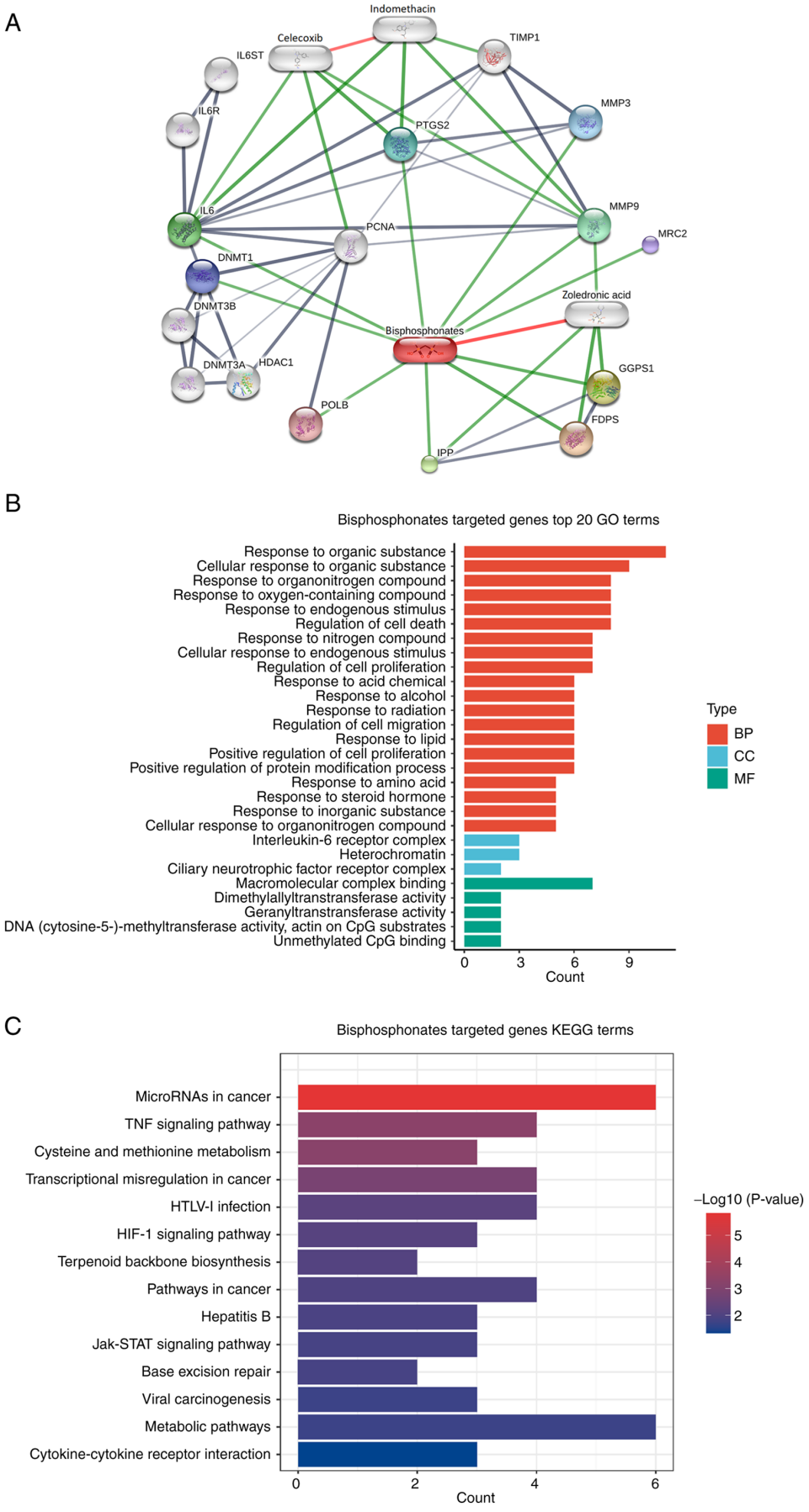

Figure 3. Predicted bisphosphonates partners and interaction network. (A) Bisphosphonates-interacting proteins were screened and the interaction networks were constructed using Chemical-Protein Interaction Networks database. Predicted bisphosphonates targets were subjected to functional annotation using ggplot2 package of R language. Top 20 (B) GO terms and (C) KEGG pathways. GO, Gene Ontology; KEGG, Kyoto Encyclopedia of Genes and Genomes; BP, biological process; CC, cellular component; MF, molecular function.

Table I. Shared Kyoto Encyclopedia of Genes and Genomes pathway and involved genes.

Term	P-value	Gene
Pathways in cancer	0.0189	FH, RALB, FLT3, LAMA4, FOXO1, EGFR, CDC42, CCND1, AKT3, DVL1, TCEB2, EP300, VHL, RAC1, WNT1, PRKACA, APPL1, JUN, DAPK2, FLT3LG, MITF, NFKB2, BMP4, NFKBIA, PLCB3, RARA, CTNNB1
HIF-1 signaling pathway	0.0548	CAMK2B, ANGPT1, INSR, AKT3, EP300, HMOX1, TCEB2, VHL, EGFR,
Viral carcinogenesis	0.0594	CAMK2B, ANGPT1, INSR, AKT3, EP300, HMOX1, TCEB2, VHL, EGFR, JUN, HIST1H2BO, SYK, ACTN2, ACTN1, RBPJ, NFKB2, CDC42, POLB, NFKBIA, CCND1, HIST1H4G, EP300, RAC1, PRKACA
HTLV-I infection	0.0812	MAP3K3, JUN, IL1R2, NFKB2, POLB, NFKBIA, HLA-DMB, CCND1, AKT3, DVL1, EP300, CTNNB1, TLN2, TCF3, SLC25A5, WNT1, PRKACA, MAP3K3, JUN, IL1R2, NFKB2, POLB, NFKBIA, HLA-DMB, CCND1, AKT3, DVL1, EP300, CTNNB1, TLN2, TCF3, SLC25A5, WNT1, PRKACA

of 'response to organic substance' and 'cellular response to organic substance', cellular components were associated with 'IL-6 receptor complex' and 'heterochromatin' and molecular functions were associated with 'macromolecular complex binding' (Fig. 3B). In addition, these proteins were involved in KEGG pathways of 'TNF-α signaling', 'cysteine metabolism' and 'methionine metabolism' (Fig. 3C). Overall, these results indicated a relationship between bisphosphonates and immunoregulation.

Identification of shared KEGG pathways between bisphosphonate targets and DEGs in PMO. Next, common KEGG pathways between DEGs in PMO and bisphosphonate partners were intersected, which yielded four pathways (Fig. 4A), including 'pathways in cancer', 'HIF-1 signaling pathway', 'human T-cell leukemia virus 1 infection' and 'viral carcinogenesis' (Fig. S1). A total of 42 DEGs in PMO were involved in these common KEGG pathways (Table I). The shared pathways mostly focused on cancer pathways, which suggested that PMO was related to proliferation-related signaling pathways.

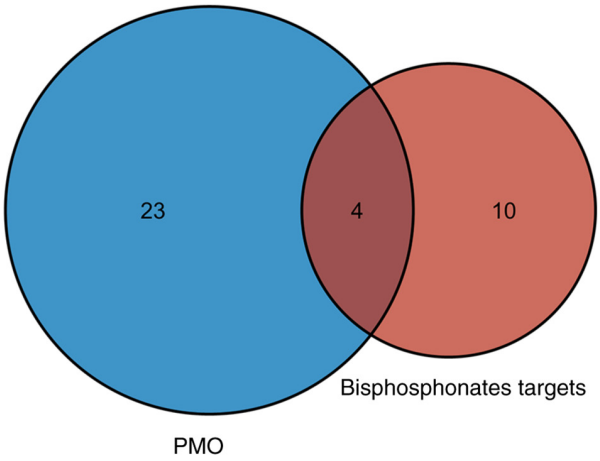

Figure 4. Identification of shared KEGG pathways between bisphosphonates targets and PMO. Venn diagram of shared KEGG pathways between bisphosphonates targets and differentially expressed genes in PMO. KEGG, Kyoto Encyclopedia of Genes and Genomes; PMO, postmenopausal osteoporosis.

PPI network of shared KEGG pathways and identification of hub genes. The 42 genes of the common KEGG pathways were used to construct a PPI network using Cytoscape software (Fig. 5A). MCODE Cytoscape App was used to integrate neighbors and density and identified 10 hub genes, including *WNT1, AKT3,* disheveled segment polarity protein 1 *(DVL1),* cyclin D1 *(CCND1),* H2B clustered histone 17 *(HIST1H2BO), JUN, EGFR, RAC1,* actinin α1 *(ACTN1)* and *ACTN2* (Fig. 5B). Among these, *WNT1, RAC1, HIST1H2BO, ACTN2* and *EGFR* were upregulated and *AKT3, DVL1, CCND1, JUN* and *ACTN1* were downregulated in PBMCs from patients with low BMD. Overall, some hub genes were established, and further identification was required.

AKT3 and RAC1 are critical genes in regulation of osteoclast formation. To determine the involvement of hub genes in osteoclast formation, THP-1 cells were treated with M-CSF and sRANKL for 3 and 5 days to induce differentiation of osteoclasts. When the majority of THP-1 cells formed a multi-nucleated fused cluster, which indicated the formation of osteoclasts (Fig. 6A and B), cells were harvested for RT-qPCR analysis. *AKT3, CCND1, EGFR* and *RAC1* were significantly upregulated, while *WNT1, JUN* and *DVL1* were downregulated and *ACTN1, HIST1H2BO* and *ACTN2* were unaffected during differentiation of osteoclasts (Fig. 6C-L). Among these, *AKT3* and *RAC1* were the most differentially expressed genes and may be involved in the regulation of osteoclast differentiation.

Inhibition of AKT3 and RAC1 enhances the inhibitory effect of bisphosphonates on osteoclasts. Bisphosphonates prevent bone loss by decreasing osteoclast activity and promoting osteoclast apoptosis (8). Cell viability assay showed that pamidronate, a commonly used bisphosphonate, dose-dependently inhibited viability of THP-1 cells and significant inhibition was observed at doses ≥10 μM (Fig. 7A). Compared with the induced differentiation group (sRANKL + M-CSF group), pamidronate at a dose of 5 μM significantly inhibited the differentiation of THP-1 cells into osteoclasts (Fig. 7C and D). Therefore, 5 μM pamidronate was used to inhibit osteoclast

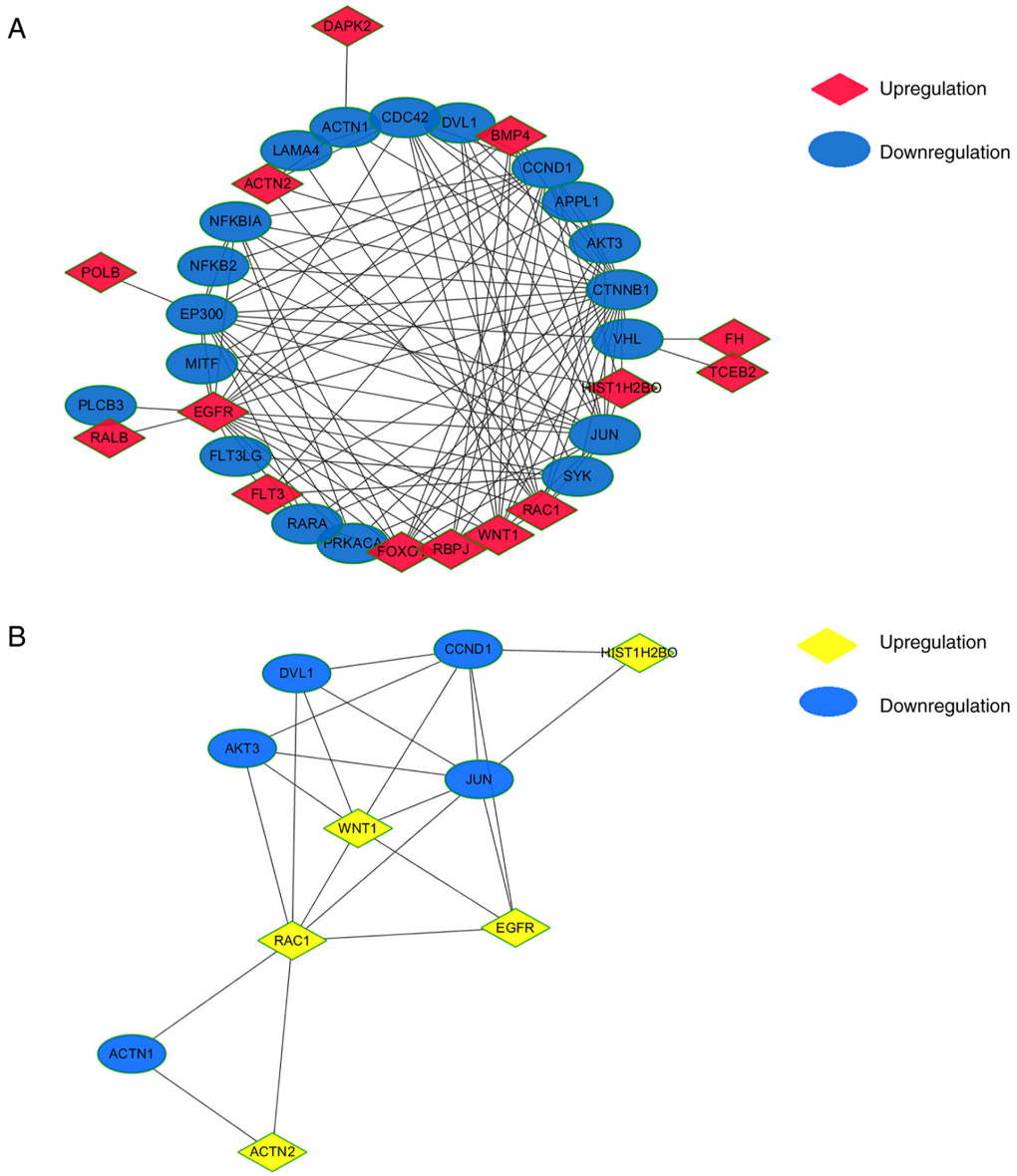

Figure 5. PPI network of shared KEGG pathways and identification of hub genes. (A) All 42 genes of the common KEGG pathways were used to construct PPI network. (B) Hub genes were calculated by the MCODE module of Cytoscape software. PPI, protein-protein interaction; KEGG, Kyoto Encyclopedia of Genes and Genomes.

differentiation from THP-1 cells and 10 μM was used for apoptosis analysis.

To assess whether AKT3 and RAC1 interfere with the effect of bisphosphonates on differentiation and activity of osteoclasts, siRNAs were used to knock down expression of AKT3 and RAC1 in THP-1 cells prior to pamidronate treatment. The results demonstrated that compared with NC, siRNA3 of AKT3 and siRNA1-3 of RAC1 interfered with the expression levels of AKT3 and RAC1, respectively. Among the three siRNAs of RAC1, siRNA3 had the most obvious effect (Fig. 7B). Knockdown of *AKT3* and *RAC1* significantly reduced the nuclear fusion of THP-1 cells compared with pamidronate treatment group, indicating that knockdown of AKT3 and RAC1 enhanced the blocking effect of pamidronate on osteoclast differentiation (Fig. 7C and D). Furthermore, siRNA of *AKT3* and *RAC1* significantly enhanced pamidronate-induced apoptosis of THP-1 cells (Fig. 7E and F). The effect of *AKT3* siRNA was notably stronger than that of *RAC1* siRNA. These data indicated that inhibition of AKT3 and RAC1 gene expression inhibited osteoclast differentiation and promoted the apoptosis-inducing effect of bisphosphonates.

Discussion

PMO is a common disease, and approximately one-third of women aged 60-70 years have osteoporosis worldwide and nearly one-third of women >50 years of age develop osteoporotic fractures (3), but the underlying mechanisms remain unclear. The present study performed differential gene expression analysis using a publicly available GEO dataset and identified DEGs between PBMCs of patients with PMO with high and low BMD. STITCH database was used to mine proteins that interact with bisphosphonates. Pathway enrichment data of the two analyses was combined, common

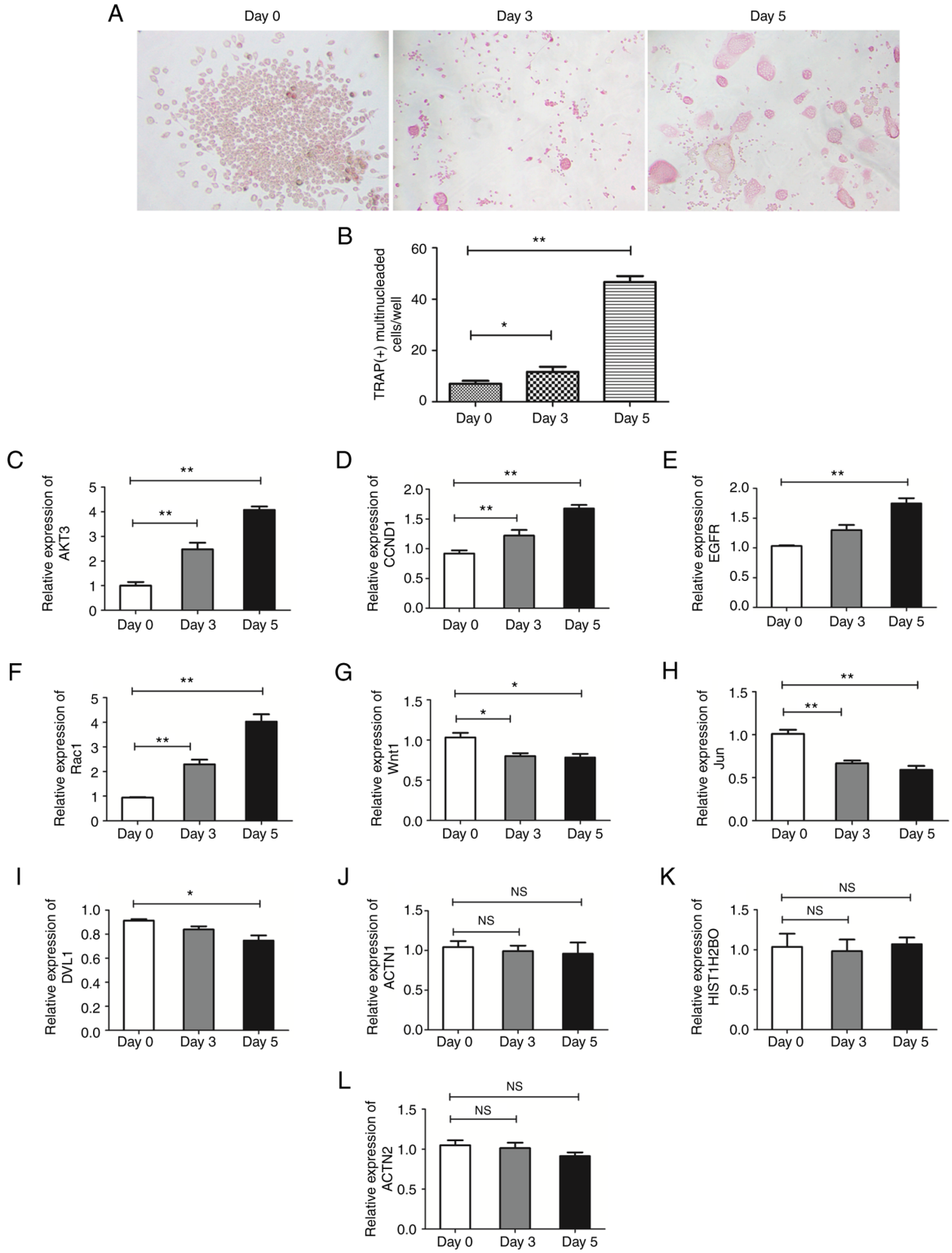

Figure 6. Expression of hub genes in osteoclasts. THP-1 cells were induced into osteoclasts for 3 and 5 days. (A) The morphology was observed and (B) the number of nuclei of multinuclear osteoclasts was counted to calculate the rate of multinuclear osteoclasts.. Expression of (C) *AKT3*, (D) *CCND1*, (E) *EGFR*, (F) *RAC1*, (G) *WNT1*, (H) *JUN*, (I) *DVL1*, (J) *ACTN1*, (K) *HIST1H2BO* and (L) *ACTN2* were assessed by quantitative PCR respectively. Magnification, x200. Data are presented as the mean ± SD. The experiments were repeated three times. *P<0.05, **P<0.01. CCND1, cyclin D1; DVL1, disheveled segment polarity protein 1; ACTN, actinin α; HIST1H2BO, H2B clustered histone 17; NS, not significant.

enriched signaling pathways were screened and two key hub genes, *AKT3* and *RAC1*, were identified. Finally, *in vitro* osteoclast formation model demonstrated that inhibiting *AKT3* and *RAC1* expression enhanced the inhibitory effect of bisphosphonates on osteoclast activation and differentiation.

Previous studies have analyzed DEGs of patients with PMO (16,17). The present study focused on gene expression of PBMCs in patients with PMO because osteoclasts are differentiated from PBMCs (18). Certain studies have shown that the RANKL signaling pathway is highly activated in

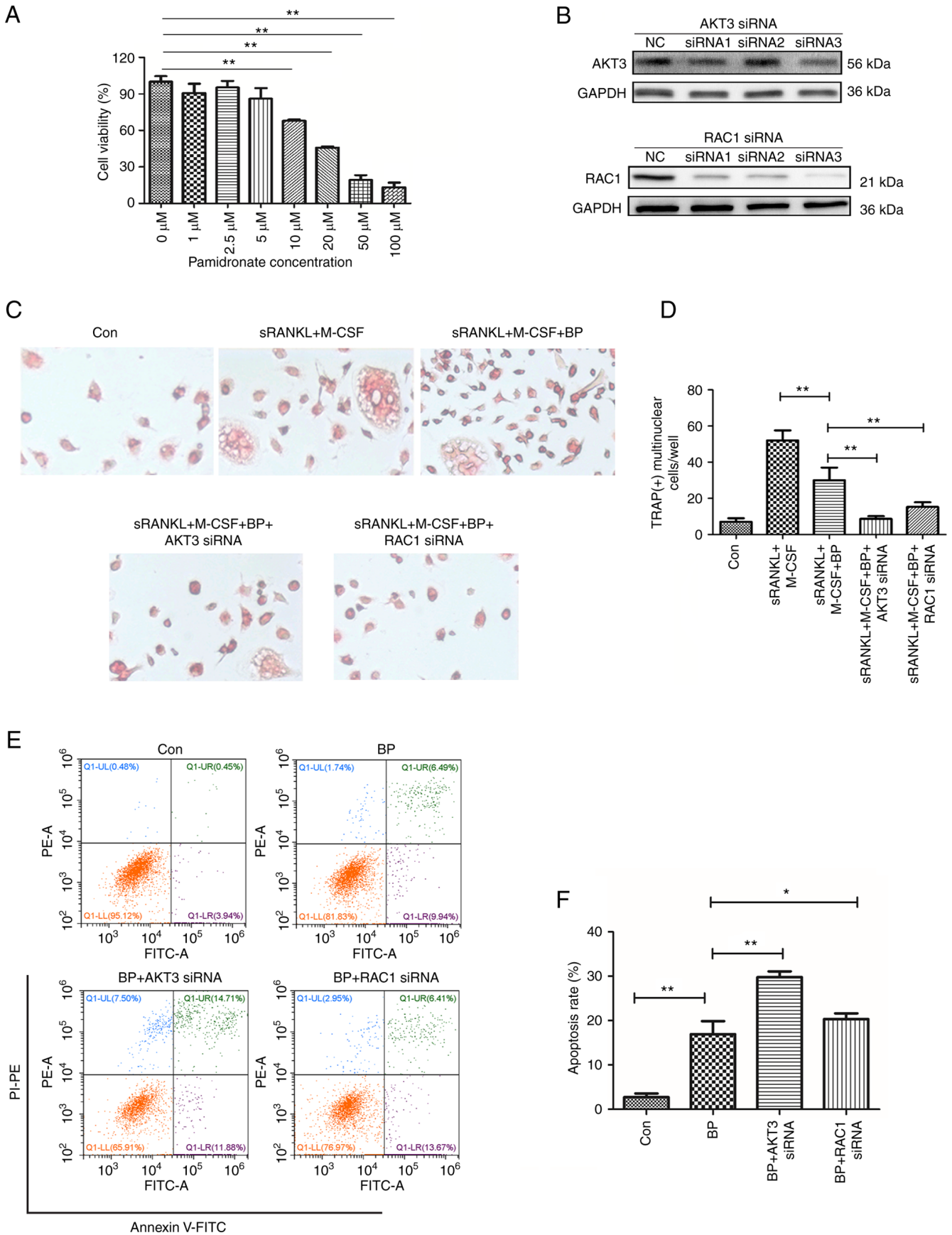

Figure 7. Inhibition of AKT3 and RAC1 enhances the inhibitory effect of BP on osteoclasts. (A) THP-1 cells were treated with pamidronate for 24 h, followed by cell viability assay using CCK-8 reagent. (B) THP-1 cells were transfected with AKT3 or RAC1 siRNA and the cells were harvested for western blotting analysis 48 h after transfection. (C) Effect of AKT3 or RAC1 siRNA on osteoclast formation. (D) Number of nuclei of multinuclear osteoclasts was counted and the rate of multinuclear osteoclasts was calculated. The apoptosis of THP-1 cells was (E) detected by flow cytometry and (F) quantified. Data are presented as the mean ± SD. The experiments were repeated three times. *P<0.05, **P<0.01. Magnification, x200. BP, bisphosphonates; NC, negative control; si, small interfering; Con, control; sRANKL, soluble receptor activator of NF-κB ligand; M-CSF, macrophage-colony-stimulating factor.

PBMCs of patients with PMO, suggesting involvement of PBMCs in the progression of PMO (19,20). The primary effect of bisphosphonates is to inhibit osteoclast activation, thereby preventing bone loss (8). Therefore, it was hypothesized that the gene expression profile of PBMCs may be used to delineate the association between bisphosphonates and osteoporosis.

Firstly, the GEO dataset was analyzed and results demonstrated a total of 290 DEGs between the low BMD patient and high BMD patient. The functional annotation of DEGs indicated that most DEGs were closely associated with hormone-related signaling pathways, DNA replication and biosynthesis, which is in accordance with the known pathogenesis of PMO, which involves dysregulation of osteoclast-associated molecules and downregulation of estrogen (21). Next, by integrating bioinformatics data of the aforementioned databases, four common KEGG pathways were identified; three were associated with occurrence and development of tumors, including 'pathways in cancer', 'HIF-1 signaling pathway' and 'viral carcinogenesis'. This indicated that certain activated signaling molecules involved in occurrence and development of PMO may exhibit crosstalk with oncogenic signaling, which has been reported in previous studies (22,23). For example, Zhong *et al* (22) showed that HIF-1 signaling is involved in the formation of PMO and Yu *et al* (23) found that the tumor suppressor P53 serves a key role in the progression of osteoporosis. Here, cancer-associated signaling pathways primarily involved biological processes such as 'proliferation' and 'differentiation'. This suggested that the occurrence of PMO is associated with proliferation and differentiation of osteoclasts.

Hub genes of the four common signaling pathways were analyzed and *WNT1, AKT3, DVL1, CCND1, HIST1H2BO, JUN, EGFR, RAC1, ACTN1* and *ACTN2* were screened out. These hub genes are primarily involved in the processes of cell proliferation and differentiation (24-31). Some genes are also reported to be involved in the formation of osteoclasts (32,33).

In addition to bioinformatics analysis, *in vitro* experiments were performed to verify the expression of the aforementioned hub genes during osteoclast differentiation. *AKT3, CCND1, EGFR* and *RAC1* were significantly upregulated, while *WNT1, JUN* and *DVL1* were downregulated during differentiation of THP-1 cells into osteoclasts. However, in the GEO dataset, expression levels of *WNT1, RAC1, HIST1H2BO, ACTN2* and *EGFR* were upregulated, while those of *AKT3, DVL1, CCND1, JUN* and *ACTN1* were downregulated in patients with PMO with low BDM. The present results showed that only four hub genes showed an expression pattern consistent with that in patients with PMO, indicating that PMO is a complex and dynamic process (34).

AKT3 and *RAC1*, which are upregulated during osteoclast differentiation, were selected for functional analysis. The inhibitory effects of bisphosphonates on osteoclasts were significantly enhanced when *AKT3* and *RAC1* expression was knocked down, which not only decreased differentiation of osteoclasts but also increased apoptosis of monocytes. Therefore, *AKT3* and *RAC1* may be promising targets for enhancing the therapeutic effect of bisphosphonates on PMO.

The association between Rac1 and PMO has previously been reported (35,36). Multiple studies have shown that activation of Rac1 promotes osteoclastogenesis (37-39); therefore, Rac1 may be an effective target for the prevention and treatment of PMO. The present results are consistent with previous findings (37-39), indicating that screening hub genes by bioinformatics combined with target prediction of drugs is feasible. To the best of our knowledge, there are no previous reports on the association between Akt3 and PMO or osteoclast activation. Therefore, the present study provided novels insights into the molecular mechanism of PMO.

The present study had certain limitations. First, only one dataset was used in the analysis, which may not reflect the gene expression pattern of PBMCs in PMO. Second, only an *in vitro* osteoclast differentiation model was used; the present findings need to be validated *in vivo*.

In summary, the present study identified *AKT3* and *RAC1* as two novel key genes in PMO via combined analysis of a GEO dataset of patients with PMO and the STITCH database. The present data provided a new avenue for understanding the mechanism of PMO and improving the therapeutic efficacy of bisphosphonates.

Acknowledgements

Not applicable.

Funding

This study was supported by The Tribology Science Fund of State Key Laboratory of Tribology (project name, Preparation and Tribological Properties of self-healing hydrogel materials for artificial joint interface; grant no. SKLTKF21B04).

Availability of data and materials

The datasets used and/or analyzed during the current study are available from the corresponding author on reasonable request.

Authors' contributions

SX and YW designed the study. LZ performed bioinformatics analysis and wrote the manuscript. XL performed experiments *in vitro* and took part in the manuscript writing. CW, WD, JZ and LF performed experiments. QF analyzed the experimental data. SX and YW confirm the authenticity of all the raw data. All authors have read and approved the final manuscript.

Ethics approval and consent to participate

Not applicable.

Patient consent for publication

Not applicable.

Competing interests

The authors declare that they have no competing interests.

References

1. Arceo-Mendoza RM and Camacho PM: Postmenopausal osteoporosis: Latest guidelines. Endocrinol Metab Clin North Am 50: 167-178, 2021.

2. McNamara LM: Osteocytes and estrogen deficiency. Curr Osteoporos Rep 19: 592-603, 2021.
3. Baccaro LF, Conde DM, Costa-Paiva L and Pinto-Neto AM: The epidemiology and management of postmenopausal osteoporosis: A viewpoint from Brazil. Clin Interv Aging 10: 583-591, 2015.
4. Manolagas SC: Birth and death of bone cells: Basic regulatory mechanisms and implications for the pathogenesis and treatment of osteoporosis. Endocr Rev 21: 115-137, 2000.
5. Fujikawa Y, Quinn JM, Sabokbar A, McGee JO and Athanasou NA: The human osteoclast precursor circulates in the monocyte fraction. Endocrinology 137: 4058-4060, 1996.
6. Cohen-Solal ME, Graulet AM, Derme MA, Gueris J, Baylink D and de Vernejoul MC: Peripheral monocyte culture supematants of menopausal women can induce bone resorption: Involvement of cytokines. J Clin Endocrinol Metab 77: 1648-1653, 1993.
7. Dera AA, Ranganath L, Barraclough R, Vinjamuri S, Hamill S, Mandourah AY and Barraclough DL: Altered levels of mRNAs for calcium-binding/associated proteins, Annexin A1, S100A4, and TMEM64, in peripheral blood mononuclear cells are associated with osteoporosis. Dis Markers 2019: 3189520, 2019.
8. Endo Y, Funayama H, Yamaguchi K, Monma Y, Yu Z, Deng X, Oizumi T, Shikama Y, Tanaka Y, Okada S, *et al*: Basic studies on the mechanism, prevention, and treatment of osteonecrosis of the jaw induced by bisphosphonates. Yakugaku Zasshi 140: 63-79, 2020 (Article in Japanese).
9. Ihn HJ, Lee D, Lee T, Kim SH, Shin HI, Bae YC, Hong JM and Park EK: Inhibitory effects of kp-a159, a thiazolopyridine derivative, on osteoclast differentiation, function, and inflammatory bone loss via suppression of rankl-induced map kinase signaling pathway. PLoS ONE 10: e0142201, 2015.
10. Livak KJ and Schmittgen TD: Analysis of relative gene expression data using real-time quantitative PCR and the 2(-Delta Delta C(T)) method. Methods 25:402-408, 2001.
11. Dutta P, Zhang L, Zhang H, Peng Q, Montgrain PR, Wang Y, Song Y, Li J and Li WX: Unphosphorylated STAT3 in heterochromatin formation and tumor suppression in lung cancer. BMC Cancer 20: 145, 2020.
12. Lithgow KV, Church B, Gomez A, Tsao E, Houston S, Swayne LA and Cameron CE: Identification of the neuroinvasive pathogen host target, LamR, as an endothelial receptor for the treponema pallidum adhesin Tp0751. mSphere 5: e00195-20, 2020.
13. Huang da W, Sherman BT and Lempicki RA: Systematic and integrative analysis of large gene lists using DAVID bioinformatics resources. Nat Protoc 4: 44-57, 2009.
14. Wang J, Liu H, Xie G, Cai W and Xu J: Identification of hub genes and key pathways of dietary advanced glycation end products-induced non-alcoholic fatty liver disease by bioinformatics analysis and animal experiments. Mol Med Rep 21: 685-694, 2020.
15. Guimaraes HI, Santana RH, Silveira R, Pinto OH, Quirino BF, Barreto CC, Bustamante MM and Krüger RH: Seasonal variations in soil microbiota profile of termite (syntermes wheeleri) mounds in the Brazilian tropical savanna. Microorganisms 8: 1482, 2020.
16. Yang C, Ren J, Li B, Jin C, Ma C, Cheng C, Sun Y and Shi X: Identification of gene biomarkersin patients with postmenopausal osteoporosis. Mol Med Rep 19: 1065-1073, 2019.
17. Liu T, Huang J, Xu D and Li Y: Identifying a possible new target for diagnosis and treatment of postmenopausal osteoporosis through bioinformatics and clinical sample analysis. Ann Transl Med 9: 1154, 2021.
18. Salamanna F, Maglio M, Borsari V, Giavaresi G, Aldini NN and Fini M: Peripheral blood mononuclear cells spontaneous osteoclastogenesis: Mechanisms driving the process and clinical relevance in skeletal disease. J Cell Physiol 231: 521-530, 2016.
19. Jin H, Yao L, Chen K, Liu Y, Wang Q, Wang Z, Liu Q, Cao Z, Kenny J, Tickner J, *et al*: Evodiamine inhibits RANKL-induced osteoclastogenesis and prevents ovariectomy-induced bone loss in mice. J Cell Mol Med 23: 522-534, 2019.
20. Chen X, Li J, Ye Y, Huang J, Xie L, Chen J, Li S, Chen S and Ge J: Association of cardiotrophin-like cytokine factor 1 levels in peripheral blood mononuclear cells with bone mineral density and osteoporosis in postmenopausal women. BMC Musculoskelet Disord 22: 62, 2021.
21. Li L and Wang Z: Ovarian aging and osteoporosis. Adv Exp Med Biol 1086: 199-215, 2018.
22. Zhong H, Cao C, Yang J and Huang Q: Research on relationship of HIF-1 signaling pathway and postmenstrual osteoporosis. Sichuan Da Xue Xue Bao Yi Xue Ban 48: 862-868, 2017 (In Chinese).
23. Yu T, You X, Zhou H, Kang A, He W, Li Z, Li B, Xia J, Zhu H, Zhao Y, *et al*: p53 plays a central role in the development of osteoporosis. Aging (Albany NY) 12: 10473-10487, 2020.
24. Wei W, He HB, Zhang WY, Zhang HX, Bai JB, Liu HZ, Cao JH, Chang KC, Li XY and Zhao SH: miR-29 targets Akt3 to reduce proliferation and facilitate differentiation of myoblasts in skeletal muscle development. Cell Death Dis 4: e668, 2013.
25. Castro-Piedras I, Sharma M, den Bakker M, Molehin D, Martinez EG, Vartak D, Pruitt WM, Deitrick J, Almodovar S and Pruitt K: DVL1 and DVL3 differentially localize to CYP19A1 promoters and regulate aromatase mRNA in breast cancer cells. Oncotarget 9: 35639-35654, 2018.
26. Wang LJ and Cai HQ: Let-7b downgrades CCND1 to repress osteogenic proliferation and differentiation of MC3T3-E1 cells: An implication in osteoporosis. Kaohsiung J Med Sci 36: 775-785, 2020.
27. He Y, Cao Y, Wang X, Jisiguleng W, Tao M, Liu J, Wang F, Chao L, Wang W, Li P, *et al*: Identification of hub genes to regulate breast cancer spinal metastases by bioinformatics analyses. Comput Math Methods Med 2021: 5548918, 2021.
28. Koyuturk M, Ersoz M and Altiok N: Simvastatin induces proliferation inhibition and apoptosis in C6 glioma cells via c-jun N-terminal kinase. Neurosci Lett 370: 212-217, 2004.
29. Abe S, Ueno M, Nishitani M, Akamatsu T, Sato T, Shimoda M, Kanaoka H, Nii Y, Yamasaki H and Yuasa K: Citrus sudachi peel extract suppresses cell proliferation and promotes the differentiation of keratinocytes through inhibition of the EGFR-ERK signaling pathway. Biomolecules 10: 1468, 2020.
30. Gahankari A, Dong C, Bartoletti G, Galazo M and He F: Deregulated Rac1 activity in neural crest controls cell proliferation, migration and differentiation during midbrain development. Front Cell Dev Biol 9: 704769, 2021.
31. Peng W, Liu Y, Qi H and Li Q: Alpha-actinin-4 is essential for maintaining normal trophoblast proliferation and differentiation during early pregnancy. Reprod Biol Endocrinol 19: 48, 2021.
32. Song C, Guo Y, Chen F and Liu W: LncRNA MALAT1 promotesosteogenic differentiation through the miR-217/AKT3 axis: A possible strategy to alleviate osteoporosis. J Gene Med 24:e3409, 2022.
33. Sharma A, McAfee J, Wang L, Cook E, Ababneh E and Bergfeld WF: Utility of Cyclin D1 immunostaining in cutaneous xanthogranuloma. Am J Dermatopathol 43: e141-e145, 2021.
34. Korsić M: Pathophysiology of postmenopausal osteoporosis. Reumatizam 53: 32-35, 2006 (In Croatian).
35. Li J, Li X, Liu D, Hamamura K, Wan Q, Na S, Yokota H and Zhang P: eIF2α signaling regulates autophagy of osteoblasts and the development of osteoclasts in OVX mice. Cell Death Dis 10: 921, 2019.
36. Magalhaes JK, Grynpas MD, Willett TL and Glogauer M: Deleting Rac1 improves vertebral bone quality and resistance to fracture in a murine ovariectomy model. Osteoporos Int 22: 1481-1492, 2011.
37. Gao L, Kong L and Zhao Y: The regulatory role of Rho GTPases and their substrates in osteoclastogenesis. Curr Drug Targets 22: 1064-1070, 2021.
38. Wang Y, Belsham DD and Glogauer M: Rac1 and Rac2 in osteoclastogenesis: A cell immortalization model. Calcif Tissue Int 85: 257-266, 2009.
39. Wang Y, Lebowitz D, Sun C, Thang H, Grynpas MD and Glogauer M: Identifying the relative contributions of Rac1 and Rac2 to osteoclastogenesis. J Bone Miner Res 23: 260-270, 2008.